Midbrain somatostatin-expressing cells control pain-suppression during defensive states

Nanci Winke[1,2§✉], Frank Aby[3§], Daniel Jercog[1,2§], Thomas Bienvenu[1,2,4], Coline Riffault[1,2], Rabia Bouali-Benazzouz[3], Juliette Viellard[1,2,3], Delphine Girard[1,2], Zoé Grivet[3], Marc Landry[3], Laia Castell[5], Emmanuel Valjent[5], Stephane Valerio[1,2]*, Pascal Fossat[3]* and Cyril Herry[1,2*✉]

[1]*Univ. Bordeaux, Neurocentre Magendie, U1215, 146 Rue Léo-Saignat, 33077 Bordeaux, France*

[2]*INSERM, Neurocentre Magendie, U1215, 146 Rue Léo-Saignat, 33077 Bordeaux, France.*

[3]*Interdisciplinary Institute for Neuroscience (IINS, CNRS UMR 5297), University of Bordeaux, Bordeaux Cedex, France.*

[4]*Centre de Référence Régional des Pathologies Anxieuses et de la Dépression, Pôle de Psychiatrie Générale et Universitaire, Centre Hospitalier Charles Perrens, Bordeaux, France.*

[5]*Université de Montpellier, Institut de génomique fonctionnelle (IGF), CNRS, Inserm, 141 rue de la Cardonille, 34094 Montpellier, France.*

§ shared authorship
* shared seniority
✉ corresponding authors: nanci.winke@inserm.fr; cyril.herry@inserm.fr

Abstract

Upon threatening situations, animals exhibit a broad range of behavioral and autonomic responses. As such, a crucial adaptive response is the inhibition of pain to facilitate relevant defensive behaviors that promote survival. Whereas the structures and mechanisms involved in fear and pain behavior are well documented, little is known about the precise neuronal mechanisms mediating the emotional regulation of endogenous pain-suppression. Here we used a combination of behavioral, anatomical, optogenetic, and electrophysiological approaches to investigate the role of that somatostatin-expressing cells in the ventrolateral periaqueductal gray matter (SST^+ vlPAG cells) in the control of analgesia induced during defensive states. Our data indicate that the optogenetic inhibition of SST^+ vlPAG cells

promotes analgesia irrespective of animal's defensive state. In contrast, the optogenetic activation of long-range SST$^+$ vlPAG cells that project to the rostral ventromedial medulla (RVM) abolishes the analgesia mediated by fear behavior. Together these results identify a novel circuit mechanism composed of long-range SST$^+$ vlPAG cells projecting to the RVM that regulate analgesia elicited during defensive states.

Introduction

During threatening situations, the inhibition of pain is an essential adaptive response that can be crucial to promote self-preservation[1–4]. The inhibition of pain responses to a stimulus that would typically elicit pain is defined as analgesia[5]. In addition, previous studies have described that a fearful event can reduce pain sensitivity, a phenomenon referred to as fear-conditioned analgesia (FCA)[6]. In particular, the pharmacological inactivation of the basolateral amygdala abolishes such fear-modulated analgesia, and is associated with an increase in the immediate-early gene c-Fos expression in the central amygdala and periaqueductal gray matter (PAG)[7]. The PAG is a midbrain structure receiving many cortical and subcortical inputs from brain structures involved in fear processing[8–11], projecting to the spinal cord primarily through a brainstem relay in the rostral ventromedial medulla (RVM)[12], a key structure involved in nociceptive transmission[13,14]. Indeed, the ventrolateral part of the PAG (vlPAG) is crucial for the descending control of pain[13,25] in the dorsal horn of the spinal cord (DH)[12], and several reports indicate that electrical stimulation of the vlPAG selectively inhibits responses to noxious stimuli in a variety of pain test conditions[12]. Moreover, analgesia induced upon vlPAG stimulation is opioid-dependent[15–17] and involves direct descending projections to the RVM and the DH[18–20,26]. Furthermore, previous research indicate that vlPAG activation induces analgesia through the recruitment of local GABAergic cells[21], which is

56 consistent with our knowledge of the role of the GABAergic system in the descending control of
57 pain[22,23]. Thus, the vlPAG is ideally located to allow the emotional regulation of pain behavior, yet
58 the underlying neuronal circuits and mechanisms are largely unknown. Here we investigated the
59 precise neural circuits within the vlPAG that mediates the suppression of pain behavior during
60 threatening situations. We developed a unique behavioral paradigm where a cued-elicited defensive
61 state promotes changes in pain sensitivity. Combining behavioral, anatomical, optogenetic, and
62 electrophysiological approaches, we identified a novel midbrain to brainstem circuit mechanism
63 composed of somatostatin positive (SST^+) vlPAG cells projecting to the RVM that is critically
64 involved in the suppression of pain behavior during conditioned fear states.
65

66 ## Results

67 ### Cued-fear conditioning elicits analgesia

68 To evaluate the contribution of specific vlPAG cells populations in the fear modulation of pain
69 behavior, we developed a novel cued fear-conditioned analgesia (CFCA) paradigm, consisting of
70 a pain sensitivity assay during the presentation of threat-predicting cues (**Figure 1a**). In this
71 paradigm, an initially neutral stimulus (the conditioned stimulus, CS^+) becomes associated with a
72 footshock (the unconditioned stimulus, US), whereas another neutral stimulus serves as a control
73 (CS^-). After conditioning, re-exposure to the CS^+ elicited freezing behavior, a behavioral readout
74 of associative learned fear[37] (**Figure 1b and Supplementary Figure 1a**). Following the fear
75 retrieval session, mice were submitted to the pain sensitivity assay. Mice were placed on a Hot-
76 Plate (HP) apparatus in which the floor plate temperature progressively increases while either CS^-
77 or CS^+ were concomitantly presented. Plate temperature increased, and CSs were continuously
78 played until mice displayed a nociceptive (NC) response reflecting pain behavior (**Figure 1c**),

defined by either jumping or hindpaw licking (**Figure 1d**). The detection of a NC response terminated the test session (**see Methods**).

We observed a significant delay in the NC response performance for CS^+ compared to CS^- presentations, reflecting that pain-suppression was selectively promoted by the threat-predicting CS (**Figure 1e and Supplementary Figure 1b**). This increased NC latency during CS^+ presentation could alternatively be explained by a competition between freezing and pain-related responses. However, freezing probability at the time of the NC response for CS^+ was remarkably low and comparable to CS^- levels, suggesting that CS^+ increased NC response latency was not due to competing freezing responses (**Figure 1f, see Methods**). Instead, these results suggest that fear induced by CS^+ presentations drives the increase in NC latency. Importantly, such states induced by our CFCA paradigm reflected fear associative processes (**Supplementary Figure 2**). To demonstrate a causal link between cued-fear and analgesia, mice were submitted to an extinction procedure to devaluate the CS^+-US contingency and abolish the negative emotional state during CS^+ presentations (**Figure 1g**). In these conditions, CS^+ presentation after extinction had no effects on NC response latency (**Figure 1h**). Furthermore, the absence of auditory cues or the presence of auditory cues not associated with a threat had comparable NC response latencies as those observed during CS^- presentations (**Figure 1i**). Finally, previous studies indicate that fear can lead to vasoconstriction, which could result in a redirection of the blood flow to the skeletal musculature, decreasing the temperature in the extremities of the body[24]. However, monitoring the back and tail temperature of mice submitted to the HP test did not reveal any difference between the CSs presentations, suggesting that increased latency was not due to fear-induced vasoconstriction (**Supplementary Figure 1c-e)**. Overall, our results indicate that the presence of a conditioned threat-predicting cue can selectively promote analgesia.

103 **Photostimulation of SST$^+$ vlPAG cells alters pain and fear behavior**

104 To identify the cell types in the vlPAG mediating the analgesic effect in the CFCA task, we
105 focused on GABAergic interneurons, which activity is suggested to be inhibited during analgesia
106 through μ-opioid receptor-dependent mechanisms[12,27]. Using single-molecule fluorescent in situ
107 hybridization (smFISH, **see Methods**), we confirmed that the majority of vlPAG SST mRNAs
108 were expressed in inhibitory neurons (**Supplementary Figure 3**). As such, since somatostatin-
109 expressing interneurons (SST) are the most abundant interneurons class in the vlPAG[28], we focused
110 on this cell population. Thus, to evaluate the contribution of SST$^+$ vlPAG cells in CFCA, SST-Cre
111 mice were injected in the vlPAG with a Cre-dependent AAV expressing the Channelrhodopsin
112 (ChR2), Archaerhodopsin (ArchT), or GFP while optic fibers were bilaterally implanted targeting
113 this area (**Figure 2a**). Next, mice were submitted to the CFCA task while photostimulating SST$^+$
114 cells in the vlPAG (**Figure 2b**; **see Methods**). After fear retrieval (**Figure 2c, e**; **Supplementary**
115 **Figure 4a-d**), the optogenetic activation of SST$^+$ vlPAG cells during the HP test had no effect on
116 CS$^-$ presentation, whereas the same manipulation performed during CS$^+$ blocked the increase in
117 NC response latency compared to GFP controls (**Figure 2d and Supplementary Figure 5a**). In
118 contrast, optogenetic inhibition of SST$^+$ vlPAG cells increased NC response latency for both CS$^-$
119 and CS$^+$ conditions compared to GFP controls (**Figure 2f and Supplementary Figure 5b**).
120 Importantly, these changes in NC response latencies were not due to motor or aversive effects of
121 the optogenetic manipulations, since photoactivation of SST$^+$ vlPAG cells did not induce changes
122 in distance travelled in an open field nor place aversion in a real-time place preference test
123 (**Supplementary Figure 5c-f**). In addition, we did not observe changes in fear learning or
124 expression when the footshock was replaced or paired with the SST$^+$ vlPAG cells photoactivation
125 during the fear conditioning procedure (**Supplementary Figure 6**).

126 Altogether, these experiments confirmed that SST^+ vlPAG activation did not promote pain
127 responses and instead suggested that the SST^+ vlPAG cells are key elements of an endogenous
128 pain-suppression circuit. Additionally, the optogenetic effect observed during CFCA was not due
129 to alteration of somatostatin levels in our homozygous SST-Cre mice[29], as we observed the same
130 effect in heterozygous SST-Cre mice (**Supplementary Figure 7a-d**). Finally, in contrast with
131 STT^+ vlPAG cells, the optogenetic inhibition of another important class of vlPAG inhibitory cells
132 expressing the vasoactive intestinal peptide (VIP^+) did not change the NC response latencies during
133 CS^- or CS^+ presentations (**Supplementary Figure 7e-h**).

134 Because our CFCA paradigm is dependent on fear associative processes (**Figure 1 and**
135 **Supplementary Figure 1-2**), it is possible that the optogenetic manipulation of SST^+ vlPAG cells
136 may have altered the expression of fear behavior. To control for this possibility, we optogenetically
137 activated or inhibited SST^+ vlPAG cells during a fear retrieval session following auditory fear
138 conditioning (**Figure 3a, b**). Our data indicate that whereas the optogenetic inhibition of SST^+
139 vlPAG cells had no effect on freezing behavior relative to GFP controls, their optogenetic
140 activation reduced freezing levels (**Figure 3c, d**). Altogether, our data show that the local SST^+
141 vlPAG network can modulate both fear expression and the analgesia promoted during defensive
142 states.

143

144 **Photostimulation of SST^+ vlPAG cells regulates spinal cord nociceptive transmission**

145 Consistent with our observations, previous studies found that the vlPAG is involved in fear-
146 conditioned analgesia[7]. It is conceivable that the SST^+ vlPAG cells are indeed part of a circuit
147 involved in the fear regulation of endogenous pain-suppression. To evaluate the effect of the
148 manipulation of SST^+ vlPAG cells on analgesia independently of the expression of fear behavior,
149 we evaluated the impact of SST^+ vlPAG cells manipulation on the control of nociceptive

150 transmission directly at the level of the spinal cord DH. Therefore, we performed extracellular local
151 field potential and single-unit recordings in the spinal cord DH during optogenetic stimulation of
152 SST^+ vlPAG cells in anesthetized mice (**Figure 4a**). Consistent with previous studies[30], nociceptive
153 stimulation induces early and late neuronal responses at the level of the spinal cord DH (A-
154 comprising non-nociceptive Aβ and nociceptive Aδ and C- fiber mediated, respectively; **Figure**
155 **4a**). While optogenetic activation of SST^+ vlPAG cells during paw suprathreshold electrical
156 stimulation increased the magnitude of late nociceptive field potentials, the optogenetic inhibition
157 reduced it (**Figure 4b, c**). To determine if this effect was specific to the nociceptive network, we
158 recorded wide dynamic range (WDR) cells in the DH, which receive both tactile (Aβ) and
159 nociceptive information (Aδ and C)[30]. We observed that SST^+ vlPAG cells photoactivation
160 increases both fast nociceptive (Aδ-fiber) and slow nociceptive (C-fiber) responses without
161 affecting Aβ (**Figure 4d**). Moreover, the optogenetic inhibition of SST^+ vlPAG cells specifically
162 inhibited nociceptive responses while Aβ responses remained unaffected (**Figure 4e**). In addition,
163 we performed subliminal electrical stimulations that did not elicit nociceptive neuronal responses.
164 In this condition, we observed that the removal of analgesia by the activation of SST^+ vlPAG cells
165 leads to WDR responses at latencies corresponding to nociceptive Aδ and C-fibers (**Figure 4f**).
166 Finally, the optogenetic activation of SST^+ vlPAG cells had no effect on purely tactile fast latency
167 spinal neurons (**Supplementary Figure 8**). Consistent with our optogenetic manipulations during
168 the CFCA task (**Figure 2**), these data suggest that under analgesia promoted by isoflurane,
169 activation and inhibition of SST^+ vlPAG cells increased or decreased nociceptive transmission by
170 specifically promoting pronociceptive and antinociceptive responses in the spinal cord DH,
171 respectively.
172

173 **SST$^+$ vlPAG-RVM-spinal cord pathway activation abolishes analgesia induced during**
174 **defensive states.**

175 We next evaluated whether SST$^+$ vlPAG cells mediate their analgesia modulation by contacting
176 WDR cells directly in the spinal cord or through the rostro ventromedial medulla (RVM), a
177 structure known to receive direct projections from vlPAG and mediate pain modulation[18,19] (**Figure**
178 **5a**). Anatomical tracing revealed large labelling of SST$^+$ fibers in RVM (**Figure 5b**) and only
179 sparse labelling within the spinal cord (SC; data not shown). By combining fluorogold
180 retrolabelling from the SC and GFP anterograde labelling from SST$^+$ vlPAG cells (**Figure 5c**), we
181 observed RVM cells projecting to the DH with close apposition of SST$^+$ putative boutons (**Figure**
182 **5d**), suggesting that SST$^+$ vlPAG cells project to the RVM and contact DH-projecting RVM cells.
183 Optogenetic activation of SST descending fibers above the SC has no effect on WDR neural
184 activity upon paw electrical stimulation, suggesting that SST$^+$ vlPAG long-range projections to SC
185 did not play a major role in endogenous pain-suppression (**Figure 5e**). In contrast, photoactivation
186 of SST$^+$ vlPAG inputs to the RVM increased both nociceptive (Aδ and C-fiber) responses (**Figure**
187 **5f, Supplementary Figure 9**). Altogether, these data revealed that the SST$^+$ vlPAG-RVM-DH
188 pathway mediates endogenous pain-suppression.

189 We next addressed if the SST$^+$ vlPAG-RVM-DH pathway was specific in the mediation of
190 endogenous pain-suppression induced by defensive states. Thus, SST-Cre mice were injected in
191 the vlPAG with a Cre-dependent AAV expressing the ChR2 or GFP, and a single optic fiber was
192 implanted above the RVM (**Figure 6a**). While photoactivation of the SST$^+$ vlPAG-RVM pathway
193 promoted nociception (**Figure 5f**), it did not impacted fear expression as freezing levels remained
194 unchanged (**Figure 6b**). Consistently, activation of the SST$^+$ vlPAG-RVM pathway during CFCA
195 had no impact on CS$^-$ presentation, whereas the same manipulation performed during CS$^+$ blocked

196 the increase in NC response latency compared to GFP controls (**Figure 6c, d**). Overall, these data
197 suggest the existence of two populations of SST^+ vlPAG cells mediating fear expression and
198 analgesia induced by defensive states. (**Figure 6e**). Altogether, our results indicate that the SST^+
199 vlPAG-RVM-DH pathway is critically involved in the analgesia induced during defensive states.
200

201 ## Discussion

202 In this study, we established that SST^+ vlPAG cells control the analgesia during defensive states.
203 Endogenous pain-suppression was mediated by long-range SST^+ vlPAG cells projecting to the
204 RVM, which in turn transmitted the pain signal to the DH of the spinal cord (**Figures 2 and 5**).
205 Finally, our data indicated that SST^+ vlPAG cells can regulate both fear expression and the
206 analgesia promoted during defensive states, and that the expression of these two behaviors can be
207 segregated by precisely targeting the SST^+ vlPAG-RVM pathway (**Figure 6**). Together these
208 results identify a novel midbrain to brainstem circuit mechanism composed of long-range SST^+
209 vlPAG cells projecting to the RVM that regulate analgesia elicited during defensive states.

210 Our observations of the involvement of vlPAG in our cued-based fear conditioned analgesia
211 paradigm are consistent with previous studies in contextual-based FCA involving this region[7]. In
212 such FCA studies[6], animals undergo contextual fear conditioning followed by pain behavior testing
213 in the same conditioning context, limiting a temporally precise elicitation of aversive states.
214 Instead, our behavioral paradigm goes beyond these limitations by promoting defensive states
215 through a cued conditioned stimulus, advancing toward temporal-specific manipulations such as
216 optogenetics, and allowing us to study the phenomena with a within-subject experimental design
217 by subsequent $CS^{+/-}$ presentations. Nevertheless, since the circuits involved in contextual and cued
218 fear may differ[31,32], this might also imply different circuits involved in the emotional modulation

219 of pain-suppression behavior. To our knowledge, this is the first demonstration of a cued fear-
220 conditioned analgesia model in rodents. Addressing possible differences in the circuitry involved
221 in contextual and cued fear-induced analgesia will require further investigation.

222 Our observation that the photoactivation of SST^+ vlPAG cells not only abolished the analgesia
223 during defensive states but also decreased freezing expression has far-reaching functional
224 consequences. Two independent previous studies found that long-range inhibitory inputs from the
225 central medial amygdala contact inhibitory cells within the vlPAG, implicated in different roles:
226 the modulation of fear behavior[21] and nociceptive transmission[33]. Notably, both studies describe
227 the involvement of vlPAG inhibitory cells in a disinhibitory circuit mechanism of long-range
228 projecting excitatory cells as the underlying neural substrates responsible for such modulations[21,33].
229 We observed that SST^+ is the most abundant type of inhibitory cells in the vlPAG (**Supplementary**
230 **Figure 3**). Thus, it is conceivable that the SST^+ vlPAG cells are indeed part of a circuit involved
231 in the emotional regulation of endogenous pain-suppression. Notably, global manipulation of SST^+
232 vlPAG cells cannot disentangle their role in analgesia and fear behavior at the local level (**Figure**
233 **2 and 3**). Because the studies mentioned above exclusively addressed the contribution of vlPAG
234 circuits in either pain behavior[33] or fear behavior[21], these studies could have been oblivious to
235 alternative behavioral readout interpretations. Here we demonstrated that SST^+ vlPAG cells
236 projecting to the RVM are involved in the modulation of analgesia induced during defensive states
237 without impacting the behavioral expression of fear (**Figure 6**). Thus, our results suggest that fear
238 and analgesia signals rely on overlapping neuronal circuits and that the discrimination between
239 these two states could be mediated within the vlPAG network. Altogether, our data is consistent
240 with the existence of different populations of SST^+ cells within the vlPAG responsible for the
241 mediation of fear behavior and analgesia information, defined by their output connectivity.

242 The lateral inhibition model of analgesia within the PAG relies on the activation of PAG
243 excitatory cells projecting to the RVM. More precisely, in this model, analgesia is thought to occur
244 through an opioid-dependent inhibition of GABAergic cells, ultimately disinhibiting excitatory
245 cells projecting to the RVM[12,19,20]. Our data indicate that in addition to this disinhibitory
246 mechanism, analgesia is also mediated by the inhibition of a direct long-range SST^+ neurons
247 projection onto RVM cells projecting to the DH (**Figure 6**). Our results align with the parallel
248 inhibition-excitation model, where inhibitory and excitatory cells form two distinct, parallel
249 descending pathways for pain modulation[35]. Indeed, previous research demonstrated the presence
250 of an inhibitory pathway projecting throughout the PAG–RVM-spinal cord dorsal horn neuraxis[36].
251 Our results complement this study by suggesting that this previously proposed inhibitory pathway
252 is mediated by GABAergic SST^+ vlPAG cells and has a functional role in mediating analgesia.
253 We identified a novel midbrain to brainstem circuit mechanism composed of SST^+ vlPAG cells
254 that project to the RVM, which regulates analgesia during defensive states. Substantial progress
255 has been made that outlined the midbrain circuitry in endogenous pain-suppression pathway[12,23,37].
256 However, only more recently, high cortical areas have also been shown to be involved in
257 analgesia[7,38]. Previous reports describe connections between CeL and vlPAG inhibitory neurons in
258 the modulation of pain behavior[21,34]. Future work is required to elucidate as to whether the exact
259 circuit that regulates analgesia are mediated by different negative emotional states such as fear,
260 depression or stress.
261 Recent human reports reveal strong comorbidity between mood and anxiety disorders with and
262 pain-related disorders[39], suggesting that the deregulation of the circuits mediating the interplay
263 between emotional and pain behavior could be at the core of such psychiatric conditions.
264 Comprehensive knowledge about the circuits mediating the emotional regulation of pain behavior
265 is urgently needed. We identified an SST^+ cell type- and pathway- specific involvement in the

266 mechanisms that mediate the emotion-dependent regulation of pain behavior. Thus, these findings
267 may empower the development of more effective analgesic therapies by the improvement of further
268 refined pharmacological targets.
269

270 Figure Legends

271 **Figure 1. Fear modulation of pain behavior. a.** Schematic of the setup and the CFCA paradigm.
272 The paradigm consists of a discriminative auditory fear conditioning test followed by a pain
273 sensitivity assay (for details, see Methods). **b.** Average freezing values for CS^+ was higher than
274 CS^- or baseline (BL) periods during retrieval (****, $P < 0.0001$, one-way RM ANOVA, n = 12
275 mice). **c.** Example of the infrared digital thermographic camera view of a mouse during the FC HP
276 test. After 1 min context acclimatization, plate temperature steadily increases at 6 ºC per min (HP
277 start). CSs started 130 s after the HP start and continued until mice displayed an NC response
278 (licking the hindpaw or jumping). **d.** Example of assessed hindpaw licking NC response. **e.** Latency
279 of NC response on the FC HP test increased during CS^+ compared to CS^- (***, $P = 0.0005$,
280 Wilcoxon matched-pairs signed rank test, n = 12 mice). **f. Left**: dynamics of freezing probability
281 at CS onset and NC response for both CS^- and CS^+ (freezing periods for each individual mouse are
282 displayed by rows in grey; error bars display S.E.M; bin size = 0.5 s). **Right**: average freezing
283 values during 10 s after CS onset and before NC response for CS^+ were higher than CS^- only at CS
284 onset (***, $P_{onset} = 0.0015$, paired t-test, n = 12 mice). **g.** Mean freezing values during fear
285 extinction, 24 CS^+ were presented across two separate extinction sessions (joined by dashed lines).
286 Mice acquired the CS^+-US association (1st CS^+ block vs. BL/CS^- ****, $P < 0.0001$, Friedman test,
287 n = 10 mice), followed by a rapid extinction (5th & 6th block of CS^+ vs BL/CS- ns, $P > 0.05$, one-
288 way RM ANOVA). **h.** After extinction, there was no difference in the NC response latency for

289 both CSs (ns, P > 0.05, paired t-test n = 10 mice). **i.** Average NC response latencies for the different
290 HP tests. *No tone* - mice submitted to the HP test without conditioning nor tone presentation. *Tone*
291 - mice submitted to the HP test paired with unconditioned tone presentation. *CS^-/CS^+* - mice were
292 submitted to the CFCA protocol. (No tone/Tone/CS^- vs. CS^+ **, P < 0.0001, Krustal-Wallis test).
293 For exact P values and test statistics on this and all subsequent figures, see Supplementary Table
294 1.

295 **Figure 2. SST^+ cells in vlPAG mediate the fear modulation of pain behavior. a.** Sst-IRES-Cre
296 mice were bilaterally injected with viruses that expressed ChR2 (right, upper), ArchT (right,
297 bottom), or GFP (control) in SST^+ vlPAG cells. **b**. Schematics of the stimulation protocol used for
298 photoactivation of the SST^+ vlPAG cells: blue light delivered at 2 Hz with 5 ms pulse duration
299 during CSs presentation until NC response. For photoinhibition experiments, green light was
300 delivered continuously. **c, e.** Average freezing values during retrieval for ChR2- (**c**) and ArchT-
301 infected mice (**e**) and their respective GFP controls. The opsin and respective control groups were
302 pooled together because no difference was found in the conditioning level (see Supplementary
303 Figure 4). Average freezing values during CS^+ was higher than CS^- or baseline (BL) periods (****,
304 P < 0.001, one-way RM ANOVA, (**c**) n = 16 mice and (**e**) n = 23 mice). **d.** Photoactivation of SST^+
305 vlPAG cells abolished the analgesic effect induced by fear (*, P = 0.0112, opsin x CS - two-way
306 RM ANOVA, n = 7 GFP, n = 9 ChR2). The NC response latency for the CS^+ was significantly
307 different between the ChR2 and GFP groups (*, P = 0.0344, Bonferroni post-hoc test). For the
308 ChR2 group, the NC response latency during CS^+ was equivalent to the CS^- (ns, P = 0.3876,
309 Bonferroni post-hoc test). On the contrary, the NC response latency between the CSs differed for
310 the GFP group (***, P = 0.0003, Bonferroni post-hoc test). **f.** Photoinhibition of SST^+ vlPAG cells
311 increased the analgesic effect for the ArchT group when compared to the GFP (*, P = 0.0037, opsin

312 x CS - two-way RM ANOVA, n = 12 GFP, n = 11 ArchT). The NC response latency for the CS^-
313 and CS^+ was significantly different between the ArchT and GFP group (CS^-: ****, $P < 0.0001$,
314 Bonferroni post-hoc test; CS^+: *, $P = 0.0265$, Bonferroni post-hoc test). For the GFP group, the
315 latency of NC response was higher for the CS^+ trials when compared to the CS^- trials (***, $P =$
316 0.0003, Bonferroni post-hoc test), yet this was not the case for the ArchT group (ns, $P > 0.999$,
317 Bonferroni post-hoc test).

318 **Figure 3. Activation of SST^+ vlPAG cells reduced fear expression a.** Protocol for optogenetic
319 manipulation during fear retrieval. Day 1 and 2 were done as described previously for the CFCA
320 paradigm. During retrieval, there were 12 CS^+ presentations divided into three blocks. **b.** The
321 stimulation protocol used for photoactivation of the SST^+ vlPAG cells. The optogenetic
322 manipulation was done during the 2nd block of the CS^+ presentation (analogously to CFCA
323 manipulations, **Figure 2b**). **c.** Light inhibition of SST^+ vlPAG cells did not modulate freezing levels
324 (ArchT ns, $P = 0.9396$, opsin x CS two-way RM ANOVA, n = 6, GFP, n = 8). **d.** Photoactivation
325 of the SST^+ vlPAG cells had no effect on the GFP group, but it transiently decreased the freezing
326 levels for the ChR2 group (***, $P < 0.0001$, opsin x CS two-way RM ANOVA, n = 9 GFP, n = 8
327 ChR2).

328 **Figure 4. Manipulation of SST^+ vlPAG cells alters spinal cord-related pain signals. a.**
329 Schematics of *in vivo* anesthetized experiments. Extracellular local field potential and single-unit
330 recordings in the spinal cord DH were performed during optogenetic stimulation of SST^+ vlPAG
331 cells with concomitant noxious electrical paw stimulation**. b.** Example of average nociceptive field
332 potentials in the lumbar SC before (OFF), during (ON), and after (OFF) photoactivation of SST^+
333 vlPAG cells (top). Photoactivation induces a significant increase in the nociceptive fields (bottom;
334 **, $P = 0.0001$, one-way RM ANOVA, n = 8 mice). **c.** Analogous to panel b, but for photoinhibition

335 of SST^+ vlPAG cells. Photoinhibition induces a significant decrease in the nociceptive fields
336 (bottom; *, P = 0.0275, one-way RM ANOVA, n = 5 mice). **d.** Example of WDR single-unit
337 activity before and during photoactivation of SST^+ vlPAG cells (**top**). Photoactivation of SST^+
338 vlPAG cells induces a significant and global increase in WDR response to both Aδ- and C-
339 mediated nociceptive fibers (**bottom**; **, $P_{A\delta\ fiber} = 0.0022$, paired t-test, n = 11 cells; **, $P_{C\ fiber} <$
340 0.0033, paired t-test, n = 11 cells). **e.** Analogous to panel d, but for photoinhibition of SST^+ vlPAG
341 cells. Photoinhibition induces a significant and specific inhibition of WDR response to Aδ- and C-
342 fibers (**bottom**; ***,** $P_{A\delta\ fiber} = 0.0241$, ****, $P_{C\ fiber} < 0.0001$, n = 14 cells**,** Wilcoxon matched-pairs
343 signed rank test). **f.** Example traces of single-unit recordings of WDR cells with subthreshold
344 electrical stimulation accompanied by photoactivation of SST^+ vlPAG cells (**top**). The
345 photoactivation of SST^+ vlPAG cells elicits WDR response to A- and C- mediated peripheral fibers
346 (**bottom**; *, $P_{A\delta\ fiber} = 0.0156$, n = 10 cells; **, $P_{C\ fiber} = 0.0020$, n = 10 cells, Wilcoxon matched-
347 pairs signed rank test).

348 **Figure 5. SST^+ vlPAG-RVM-DH pathway activation removes analgesia. a**. Schematics of
349 possible SST^+ vlPAG circuits mediating analgesia by long-range projections directly to the SC or,
350 alternatively, by projecting to the SC via the rostral ventromedial medulla (RVM). **b.** Sst-IRES-
351 Cre mice were injected with an anterograde AAV Cre-dependent GFP virus in the vlPAG (left).
352 Example of SST fibers labelling at the level of the RVM (middle)**.** Higher magnification (right)
353 reveals putative axonic buttons in the RVM (examples indicated by white arrows). **c.** Sst-IRES-
354 Cre mice were injected concomitantly with anterograde AAV Cre-dependent GFP virus in the
355 vlPAG and retrograde fluorogold in the lumbar DH of the SC. **d.** Fluorogold positive cells (red)
356 cross SST^+ vlPAG fibers in the RVM (green). Higher magnification (**right**) shows close contacts
357 between the putative SST^+ button and $fluorogold^+$ cells or fibers (white arrows). **e.** Sst-IRES-Cre

358 mice were injected in the vlPAG with AAV Cre-dependent ChR2 virus and optic fiber placed above
359 the lumbar SC. Single-unit recordings of WDR cells while photoactivation of the SST^+ vlPAG SC
360 fibers and electrically stimulating the paw in anesthetized mice (**left**). Photoactivation of vlPAG
361 projections to SC did not affect nociceptive transmission (**right**; ns, P = 0.3683, paired t-test, n =
362 11 cells). **f.** Same experimental design as in panel e, except that the optic fiber was placed above
363 the RVM (left). Photoactivation of SST^+ vlPAG inputs to the RVM induces a significant increase
364 in WDR response to both Aδ- and C-mediated nociceptive fibers stimulation (**middle**; *, $P_{A\delta\ fiber}$ =
365 0.0346, Paired t-test, n = 10 cells; **, $P_{C\ fiber}$ = 0.0020, Wilcoxon matched-pairs signed rank test, n
366 = 10 cells). Removal of analgesia by activation of SST^+ vlPAG-RVM induces a significant increase
367 in WDR response to C-fibers responses (right; **, P = 0.0078, Wilcoxon matched-pairs signed
368 rank test, n = 9 cells).

369

370 **Figure 6. SST^+ vlPAG-RVM-SC pathway activation abolishes analgesia induced by CFCA.**
371 **a.** Sst-IRES-Cre mice were bilaterally injected with an AAV expressing ChR2 or GFP in the
372 vlPAG, and optic fibers were implanted above the RVM (left). Representative example of SST^+
373 vlPAG terminals in the RVM (right). **b.** Photoactivation of SST^+ vlPAG-RVM pathway did not
374 modulate freezing levels (ns, P = 0.6443, opsin x CS two-way RM ANOVA; CS^+ 2nd block, GFP
375 vs. ChR2 ns, P > 0.9999, Bonferroni post-hoc test, n = 7 GFP, n = 6 ChR2). **c.** Average freezing
376 values during retrieval for pooled ChR2 and GFP-infected mice (groups were pooled together since
377 no difference was found in the conditioning level). Average freezing values during CS^+ were higher
378 than CS^- or baseline (BL) periods (****, P < 0.0001, one-way RM ANOVA, n = 14 mice). **d.**
379 Photoactivation of SST^+ vlPAG-RVM pathway abolished the analgesic effect modulated by fear
380 (**, P = 0.0063, opsin x CS - two-way RM ANOVA, n = 7 GFP, n = 7 ChR2). For the ChR2 group,

381 the NC response latency during CS^+ was equivalent to the CS^- (ns, $P > 0.9999$, Bonferroni post-
382 hoc test). On the contrary, the NC response latency between the CSs differed for the GFP group
383 (****, $P < 0.0001$, Bonferroni post-hoc test). **e**. Working model schematics for SST^+ control
384 analgesia induced during defensive states. Activation of SST^+ cells in the vlPAG is associated with
385 the inhibition of fear-induced freezing behavior. Selective activation of RVM projecting SST^+
386 vlPAG cells is associated with an inhibition of analgesia induced during defensive states.
387

388 # Methods

389 **Subject details**

390 We used either male C57BL6/J mice (Janvier), heterozygous or homozygous Sst-IRES-Cre
391 mice (Jackson laboratory), or heterozygous VIP-IRES-Cre mice (Jackson Laboratory) age 8-14
392 weeks that were individually housed under a 12 h light-dark cycle and provided with food and
393 water ad libitum. All procedures were performed in accordance with standard ethical guidelines
394 (European Communities Directive 86/60-EEC) and were approved by the committee on Animal
395 Health and Care of Institut National de la Santé et de la Recherche Médicale and the French
396 Ministry of Agriculture and Forestry (agreement #A3312001).
397

398 **Behavioral apparatus**

399 ***Cued fear-conditioned analgesia*** *task* was performed in three different contexts (**Figure 1a**).
400 Context A was used for *Habituation* and *Retrieval* and consisted of a plexiglass cylinder (25 x 24
401 cm diameter) with a grey, smooth plastic floor and house lights (16 lux). Context B was used for
402 *Fear conditioning* and consisted of a square plexiglass (25 x 40 cm) with a grid floor connected to
403 a shocker (Coulbourn Instruments) and brighter house lights (40 lux). A total of 5 scrambled

404 footshocks of 1 s duration and intensity of 0.8 mA were delivered via the grid floor and served as
405 the unconditioned stimulus (US). Context A and B were cleaned, respectively, with 70% ethanol
406 or 1 % acetic acid between different mice. Both contexts contained an infrared beam detection that
407 automatically scored freezing periods, determined by no change in infrared beam crossing for at
408 least 2 s.

409 Context C was used for the *FC Hot Plate (HP) test*. A steady increase in temperature was
410 controlled by the Incremental Hot/Cold Plate Analgesia Meter (IITC) device. To restrain the mice's
411 movement, the HP apparatus had a testing surface (plate) enclosed in a square plexiglass surface
412 (20.3 x 10 x 20.5 cm) and house lights (100 lux). The mice's temperature and surroundings were
413 recorded with an infrared digital thermographic camera (Testo 885) placed ~ 50 cm above the
414 testing surface. The thermal camera had a spatial resolution of 320 × 240 pixels, a sampling rate of
415 25 Hz, and thermal sensitivity of 0.03 °C at 30 °C. The testing surface of context C was cleaned
416 with water between different mice. All three contexts were enclosed in an acoustic foam isolated
417 box with speakers mounted on the top of each compartment. The auditory conditioned stimulus
418 (CS) consists of either 7.5 kHz or white-noise 50 ms pips at 1 Hz repeated 27 times, 2 ms rise and
419 fall, and 80 dB sound pressure level.

420 ***Open field*** *task* was performed in a square plexiglass arena (36 x 36 x 25cm). A LED mounted
421 on the top-right side of the arena signalled the start and end of different epochs for offline analyses.
422 A video camera recorded from above the arena at 30 fps for offline video-tracking purposes.

423 ***Real-Time Place Preference (RTPP)*** *task* was performed in a shuttlebox consisting of a
424 plexiglass box (40 x 10 x 30 cm) with a floor grid, where a small plastic hurdle (1 cm height)
425 divided the arena into two equal compartments while infrared beams detection automatically
426 monitored the mice shuttling between compartments (Imetronic). A video camera recorded from
427 above the arena at 30 fps for offline video-tracking purposes.

428 For both the open field and RTPP task, a free user video-tracking software (idTracker: Tracking
429 individuals in a group by automatic identification of unmarked animals) together with in-house
430 codes in Matlab (The MathWorks, Inc., Natick, MA, USA) were used to analyze each condition.

431 **Behavioral paradigm**

432 ***Cued fear-conditioned analgesia (CFCA).*** C57BL6/J mice (n = 12) were habituated to the
433 context and tones (day 1). Four white-noise (CS^-) and four 7.5 kHz (CS^+) tones were presented
434 sequentially and without US reinforcement. In Fear conditioning (day 2), five CS^- and five CS^+
435 were presented in an intermingled fashion. The CS^+ presentations were paired with a mild
436 footshock (US) at tone offset, whereas the CS^- was never reinforced. The Fear retrieval session
437 (Day 3) was done 24h after conditioning and in the same context as the habituation session. As in
438 habituation, four CS^- and four CS^+ were presented sequentially and without US reinforcement
439 (**Figure 1a**).

440 Since the focus of this study was the emotional modulation of pain sensitivity, it was compulsory
441 to evaluate the associative fear levels before measuring its impact on pain sensitivity. Two indices
442 were computed: the discrimination index (DI), to assess the discrimination between CS^- and CS^+,
443 and the conditioning index (CI), which indicated the level of freezing to the tone predicting the US.
444 These indexes were calculated as follows: $DI = \frac{(Freezing\ to\ CS+)-(Freezing\ to\ CS-)}{(Freezing\ to\ CS+)+(Freezing\ to\ CS-)}$ and CI = DI ×
445 (Freezing to CS^+). Based on preliminary data, mice were only submitted to the FC HP test if DI ≥
446 0.4 & CI ≥ 0.3. Mice that did not fit the criteria were conditioned a second time. There was a
447 minimum interval of 2 h between the retrieval and the FC HP test.

448 The FC HP test consisted of two trials, one where the CS^+ was presented and another where the
449 CS^- was presented. The two trials were counterbalanced within the group. The testing surface was
450 set at 30 ºC**.** After a 60 s acclimatization period, its temperature gradually increased at 6 ºC per

451 minute (HP start). Tone presentation (CS^+ or CS^-) started 130 s after the HP start. Temperature
452 increase and tone presentation terminated concomitantly with the display of a nociception response.
453 Valid nociception readout responses included jumping or licking the hindpaw. The effect of the
454 negative emotional modulation on pain sensitivity was assessed by comparing the latency (or
455 temperature) of the NC response between the two HP trials. There was a minimum of 30 min
456 interval between the two trials for each mouse, during which mice returned to their home cage.

457 Freezing during the HP test was assessed by automatically analyzing thermographic camera
458 videos using custom scripts (available at: github.com/djercog/TestoFreez). Briefly, individual
459 video frames were binarized to define a mask for the mouse within each frame. Consecutive
460 binarized frames were then subtracted, and the number of non-zero pixels on the resultant image
461 determined if the mouse was considered immobile when below a certain threshold (defined to
462 approximate manual freezing estimation on random videos). Immobilization episodes of at least
463 0.5 s were considered as freezing periods. In contrast, non-immobilization episodes shorter than
464 0.1 s were merged together with the neighbouring detected freezing episodes.

465 ***Extinction training.*** On days 3 and 4, mice (n =10) were submitted to an extinction training
466 protocol established by Courtin et al. 2014[40]. Briefly, there were 4 CS^- and 12 CS^+, presented in a
467 non-reinforced manner (**Figure 1g**). Mice were considered as having successfully extinguished the
468 fear expression if the level of freezing in the last 4 CS^+ was not statistically different from the CS^-
469 . After fear extinction, mice were submitted to the FC HP test, using the same parameters as in the
470 CFCA paradigm.

471 ***Stability training***. The first three days consisted of the classical CFCA paradigm. On day 4,
472 mice (n = 10) repeated the protocol applied on day 3 (**Supplementary Figure 2e-i)**. All mice that
473 passed the fear conditioning criteria (DI ≥ 0.4 & CI ≥ 0.3) on day 3 were kept for the following
474 day, independent of their level of Conditioning on day 4.

475 ***Vasoconstriction assay.*** To determine if vasoconstriction was a confounding factor in the FC
476 HP test outcomes, we used a modified version of the CFCA paradigm (**Figure 1f)**. During the HP
477 test (n = 13), the temperature was not gradually increased but maintained at 30 ºC while CSs were
478 presented. The tones (CS^+ or CS^-) were presented for 120 s, and mice were kept for an additional
479 50 s before the HP trial terminated. Offline, with the infrared videos, mice's back and tail were
480 measured at 30 s intervals. For each measuring point, the temperature of three spots of the two
481 body part was averaged to create the body temperature for the back and tail for a given time point
482 and mouse.

483 ***Basal nociception assay (No tone).*** Naïve mice (n = 10) were submitted to the HP test (**Figure**
484 **1i and Supplementary Figure 2a-d)**. Each mouse underwent two identical trials. The HP test was
485 similar to the one described in the CFCA paradigm, except no tones were presented. There was a
486 minimum of 30 min interval between the two trials, during which mice returned to a restful state
487 in their home cage. Since the two trials were not significantly different, for simplification, in panel
488 i from Figure 1, the two trials were pooled together.

489 ***Tone-specific nociception assay.*** Naïve mice (n = 12) were submitted to the HP test without
490 auditory fear conditioning (**Figure 1i and Supplementary Figure 2a-d)**. Each animal underwent
491 two trials, one trial with a 7.5 kHz tone presentation and another with a WN tone presentation. The
492 tone presentation was counterbalanced. The HP test parameters were similar to the one described
493 for the CFCA, except that both tones were unconditioned. Since the two trials were not significantly
494 different, for simplification, in panel i from Figure 1, the two trials were pooled together.

495 ***Open Field assay.*** This test was used to determine the effect of optogenetic stimulation on
496 locomotion. Therefore, only mice from optogenetic experiments were submitted to this assay. Mice
497 could freely move during the entire test. The locomotion assay had a total duration of 9 min and
498 was divided into 3 min epochs. The first and third epochs were OFF periods in which no optical

499 stimulation occurred. During the second epoch, mice received photostimulation (ON period). The
500 optogenetic stimulation effect was analyzed by comparing the overall distance travelled between
501 the OFF and ON epochs (**Supplementary Figure 5c, d)**. Mice injected with GFP were used to test
502 the effect of heat and light on the stimulation itself. Mouse tracking data was extracted from video
503 recordings using idTracker[41] and imported to Matlab for further analysis using custom scripts to
504 calculate the total distance travelled during stimulation.

505 ***Real-time Place Preference assay.*** Only mice from optogenetic experiments were submitted to
506 this assay. During the entire duration of the assay, mice could freely shuttle between the two
507 compartments. Under a closed-loop stimulation, mice received photo-stimulation upon entry into
508 one of the two compartments. The stimulated compartment was counterbalanced within the group.
509 The optical stimulation effect was assessed by comparing the time spent in the stimulated
510 compartment between the ChR2 and GFP groups (**Supplementary Figure 5e, f**). Permanence time
511 in the stimulated compartment was automatically assessed by apparatus software (Imetronic).

512 **Virus injections and optogenetics**

513 For optogenetic manipulation of SST^+ cells in the vlPAG, 0.15-0.2 µL of either ChR2 (AAV5-
514 EF1a-DIO-hChR2(H134R)-EYFP, titer: $3.2x10^{12}$ - Vector Core, University of North Carolina),
515 ArchT (AAV9-CAG-FLEX-ArchT-GFP, titer: $4.7x10^{12}$ - Vector Core, University of North
516 Carolina) or GFP (AAV5-FLEX-GFP, titer: $4.5x10^{12}$ - Vector Core, University of North Carolina)
517 were bilaterally injected into the vlPAG of 8/9 weeks old Sst-IRES-Cre mice from glass pipettes
518 (tip diameter 20-30 µm) at the following coordinates relative to bregma: - 4.4 mm AP; ± 1.5 mm
519 ML; -2.45 mm DV from dura, with a 20 degrees angle. Injection coordinates for manipulating VIP^+
520 vlPAG cells were the following: - 4.4 mm AP; ± 1.35 mm ML; -2.5 mm DV from dura, with a 20
521 degrees angle.

522 At two weeks after the injections, mice were bilaterally implanted with custom-built optic fibers
523 (diameter: 200 µm; numerical aperture: 0.39; Thorlabs) above the vlPAG at the following
524 coordinates relative to bregma: i) Sst-IRES-Cre mice: - 4.4 mm AP; ± 1.0 mm ML; -1.8 mm DV
525 from dura, with a 10 degrees angle; ii) VIP-IRES-Cre mice: - 4.4 mm AP; ± 0.8 mm ML; -2.0 mm
526 DV from dura, with a 10 degrees angle. For RVM manipulations, mice were implanted at the
527 following coordinates relative to bregma: -5.8 mm AP; 0.0 mm ML; -5.2 DV from the dura. All
528 implants were secured using three stainless steel screws and Super-Bond cement (Sun Medical).
529 During surgery, long- and short-lasting analgesic agents were injected (Metacam, Boehringer;
530 Lurocaïne, Vetoquinol). After surgery, mice were allowed to recover for at least five days.
531 Afterward, mice were handled daily to familiarize themselves with being restrained for the optic
532 fibers connection. Behavioral experiments were performed at least four weeks after viral injections.
533 Only mice with correct placement of optic fibers and virus expression were included in the
534 analyses.

535 For optogenetic excitation, light stimulation consisted of blue light (473 nm, ~8-10 mW at fiber
536 tip) delivered with 2 Hz frequency and 5 ms pulse duration. In contrast, light stimulation consisted
537 of green light (532 nm, ~8-10 mW at fiber tip) delivered continuously for optogenetic inhibition.
538 For optogenetic manipulations during the CFCA paradigm of either SST^+ or VIP^+ vlPAG cells, the
539 light was delivered during the FC HP test and paired with the tone presentation.

540 Two sets of experiments were performed sequentially for stimulation during the fear
541 conditioning. First, the footshock US was replaced by optical stimulation. Then, the US became
542 the optical stimulation combined with the footshock (**Supplementary Figure 6**). For both
543 conditions, the optogenetic stimulation started 5 s before and lasted until 5 s after CS^+ offset. The
544 same mice were used for both experiments. For the manipulations during the fear retrieval, there

545 were 12 CS^+ presentations divided into blocks of 4 CS^+. The optogenetic stimulation was paired
546 with the second block of CS^+.

547 **Anatomical tracing**

548 ***Fluorogold injection.*** An incision between one to two cm was made slightly caudal to the peak
549 of the dorsal hump to expose the lumbar spinal region. The vertebra of interest was identified.
550 Then, a small incision was made between the tendons and the vertebral column on either side. The
551 vertebra was then secured using spinal adaptor clamps, and all tissue was removed from the surface
552 of the bone. Pulled borosilicate glass capillaries (Ringcaps, disposable capillary pipettes with ring
553 mark, DURAN, Hirschmann Laborgeräte, Germany) were inserted between 2 vertebrae and
554 allowed to microinject 0.5 µL of fluorogold 2% in the dorsal horn of the spinal cord on both sides.

555 ***In vivo* electrophysiology**

556 Mice were anesthetized with isoflurane 4% for induction, then 1.5% maintenance. The
557 experiment was started as soon as there was no longer any reflex. The colorectal temperature was
558 kept at 37 °C with a heating blanket. Two metal clamps were used to set the animal spine in a
559 stereotactic frame (M2E, France) for stability during electrophysiological recordings. Then, a
560 laminectomy was performed at T13-L1 to expose the lumbar part of the spinal cord. The dura mater
561 was carefully removed. Custom-made optical fibers were placed 1mm above the dorsal spinal cord
562 for optogenetic manipulations. C-fiber-evoked field potentials were recorded in the deep lamina of
563 the DH (at a depth range of 250 and 500 µm) with borosilicate glass capillaries (2 MΩ, filled with
564 NaCl 684 mM; Harvard Apparatus, Cambridge, MA, USA). Field potentials were recorded with
565 an ISODAM-amplifier (low filter: 0.1Hz to high filter: 0.1 kHz; World Precision Instruments,
566 USA) in response to electrical stimulation of the ipsilateral paw. Single unit recordings of WDR
567 DH cells were made with the same borosilicate glass capillaries mentioned above and placed in the

568 dorsal part of the spinal cord. The criterion for selecting a cell was the presence of an A-fiber-
569 evoked response (0-80 ms) followed by a C-fiber-evoked response (80-150 ms) to electrical
570 stimulation of the ipsilateral sciatic nerve.

571 The paw of the mice was stimulated by trains (every 30 s) of electrical stimulation at two times
572 the threshold for C-fibers were performed before, during, and after optogenetic stimulations with
573 an optic fiber placed above the recording site. Subthreshold stimulations were performed below
574 the threshold for C-fiber and A-fiber, respectively.

575 **Histology analyses**

576 Mice were administered a lethal dose of Exagon and underwent transcardial perfusions via the
577 left ventricle with 4% w/v paraformaldehyde (PFA) in 0.1 M PB. Following dissection, brains were
578 post-fixed for 24 h at 4°C in 4% PFA. Brain sections of 80 µm-thick were cut on a vibratome,
579 mounted on gelatin-coated microscope slides, and dried. To verify correct viral injections and optic
580 fiber location, serial 80 µm-thick slices containing the regions of interest were mounted in
581 VectaShield (Vector Laboratories) and imaged using an epifluorescence system (Leica DM 5000)
582 fitted with a 10-x dry objective. The location and the extent of the injections/infections were
583 visually controlled. Only infections targeting the vlPAG and optic fibers terminating, depending
584 on the experiment, above the vlPAG or RVM were included in the analyses.

585 **Statistics**

586 All statistics details are contained in Supplementary Table 1. Box-whisker plots indicate
587 median, interquartile range, and 5th - 95th percentiles of the distribution. All statistics are indicated
588 where used. Statistical analyses were performed with Prism software (GraphPad). We tested the
589 normality of all data with the Kolmogorov–Smirnov normality test in Prism software (GraphPad),
590 and used nonparametric statistical tests for nonnormally distributed datasets, as indicated where

591 used. No statistical methods were used to predetermine sample sizes, but sample sizes were based
592 on previous studies in our laboratory. Blinding for the opsin was done for optogenetics
593 experiments. Animals used for the CFCA paradigm that did not satisfy the DI and CI criteria after
594 two conditioning sessions were discarded from the study. Mice with an incorrect injection of the
595 opsins or misplaced location of the optic fibers were discarded. For *in vivo* electrophysiology, field
596 potentials were measured as the area above the curve in the C-fiber range (80-300 ms). Absolute
597 values were used to compare values in each condition (OFF vs. ON optogenetic manipulation). In
598 single-unit recordings, the number of A- and C-fiber induced spikes of WDR cells were measured
599 after each electrical stimulation, during, and after optogenetic manipulation. An average of the four
600 stimuli for each WDR recorded was used for statistical analysis. Outliers were removed using the
601 Tukey method.

602 No other mice were excluded. Significance levels are indicated as follows: *$p<0.05$, **$p<0.01$,
603 ***$p<0.001$, **** $p<0.0001$.

604 **Data and script availability**

605 Data supporting the findings of this study and data analysis codes are available from the
606 corresponding author on request.

607

608 ## References

609 1. Bolles, R. C. & Fanselow, M. S. A perceptual-defensive-recuperative model of fear and
610 pain. 291–323 (1980).

611 2. Rhudy, J. L. & Meagher, M. W. Fear and anxiety: divergent effects on human pain
612 thresholds. *Pain* **84,** 65–75 (2000).

613 3. Beckham, J. C. *et al.* Chronic posttraumatic stress disorder and chronic pain in vietnam
614 combat veterans. *J. Psychosom. Res.* **43,** 379–389 (1997).

615 4. Flor, H. & Grüsser, S. M. Conditioned stress-induced analgesia in humans. *Eur. J. Pain* **3,**

616 317–324 (1999).

617 5. International Association for the Study of Pain. IASP Terminology. *Iasp* (2017).

618 6. Butler, R. K. & Finn, D. P. Stress-induced analgesia. *Prog. Neurobiol.* **88,** 184–202 (2009).

619 7. Rea, K., Roche, M. & Finn, D. P. Modulation of conditioned fear, fear-conditioned
620 analgesia, and brain regional C-fos expression following administration of muscimol into
621 the rat basolateral amygdala. *J. Pain* **12,** 712–721 (2011).

622 8. Floyd, N. S., Price, J. L., Ferry, A. T., Keay, K. a & Bandler, R. Orbitomedial prefrontal
623 cortical projections to distint longitudinal columns of the periaqueductal gray in the rat. *J.*
624 *Comp. Neurol.* **422,** 556–578 (2000).

625 9. LeDoux, J. E., Iwata, J., Cicchetti, P. & Reis, D. J. Different projections of the central
626 amygdaloid nucleus mediate autonomic and behavioral correlates of conditioned fear. *J.*
627 *Neurosci.* **8,** 2517–29 (1988).

628 10. Vertes, R. P. Differential Projections of the Infralimbic and Prelimbic Cortex in the Rat.
629 *Synapse* **51,** 32–58 (2004).

630 11. Carrive, P. & Morgan, M. M. *Periaqueductal Gray - Chapter 10. The Human Nervous*
631 *System* (Elsevier, 2012). doi:10.1016/B978-0-12-374236-0.10010-0

632 12. Basbaum, A. I. & Fields, H. L. Endogenous Pain Control Systems: Brainstem Spinal
633 Pathways and Endorphin Circuitry. *Annu. Rev. Neurosci.* **7,** 309–338 (1984).

634 13. Millan, M. J. Descending control of pain. *Prog. Neurobiol.* **66,** 355–474 (2002).

635 14. Fields, H. L., Heinricher, M. M. & Mason, P. Neurotransmitters in nociceptive modulatory
636 circuits. *Annu. Rev. Neurosci.* **14,** 219–245 (1991).

637 15. Castilho, V. M., Macedo, C. E. & Brandão, M. L. Role of benzodiazepine and serotonergic
638 mechanisms in conditioned freezing and antinociception using electrical stimulation of the
639 dorsal periaqueductal gray as unconditioned stimulus in rats. *Psychopharmacology (Berl).*
640 **165,** 77–85 (2002).

641 16. Helmstetter, F. J. & Landeira-Fernandez, J. Conditional hypoalgesia is attenuated by
642 Naltrexone applied to the periaqueductal gray. *Brain Res.* **537,** 88–92 (1990).

643 17. Bellgowan, P. S. F. & Helmstetter, F. J. The role of mu and kappa opioid receptors within
644 the periaqueductal gray in the expression of conditional hypoalgesia. 83–89 (1998).

645 18. Jacquet, Y. F. The NMDA receptor: central role in pain inhibition in rat periaqueductal gray.
646 *Eur. J. Pharmacol.* **154,** 271–276 (1988).

647 19. Moreau, J. L. & Fields, H. L. Evidence for GABA involvement in midbrain control of
648 medullary neurons that modulate nociceptive transmission. *Brain Res.* **397,** 37–46 (1986).

649 20. Osborne, P. B., Vaughan, C. W., Wilson, H. I. & Christie, M. J. Opioid inhibition of rat
650 periaqueductal grey neurones with identified projections to rostral ventromedial medulla in

651 vitro. *J. Physiol.* **490,** 383–389 (1996).

652 21. Tovote, P., Esposito, M. S., Botta, P., Chaudun, F. & Jonathan, P. Midbrain circuits for
653 defensive behaviour. *Nature, Press* (2016). doi:10.1038/nature17996

654 22. Fields, H. L. State-dependent opioid control of pain. *Nat. Rev. Neurosci.* **5,** 565–75 (2004).

655 23. Lau, B. K. & Vaughan, C. W. Descending modulation of pain: the GABA disinhibition
656 hypothesis of analgesia. *Curr. Opin. Neurobiol.* **29,** 159–164 (2014).

657 24. Vianna, D. M. L. & Carrive, P. Changes in cutaneous and body temperature during and after
658 conditioned fear to context in the rat. *Eur. J. Neurosci.* **21,** 2505–2512 (2005).

659 25. Samineni, V. K. *et al.* Divergent Modulation of Nociception by Glutamatergic and
660 GABAergic Neuronal Subpopulations in the Periaqueductal Gray. *eNeuro* **4,** (2017).

661 26. Harris, J. A. Descending antinociceptive mechanisms in the brainstem: their role in the
662 animal's defensive system. *J. Physiol. Paris* **90,** 15–25 (1996).

663 27. Fields, H. State-dependent opioid control of pain. *Nat. Rev. Neurosci.* **5,** 565–75 (2004).

664 28. Smith, G. S. T. *et al.* Distribution of messenger RNAs encoding enkephalin, substance P,
665 somatostatin, galanin, vasoactive intestinal polypeptide, neuropeptide Y, and calcitonin
666 gene-related peptide in the midbrain periaqueductal grey in the rat. *J. Comp. Neurol.* **350,**
667 23–40 (1994).

668 29. Viollet, C. *et al.* Somatostatin-IRES-Cre Mice: Between Knockout and Wild-Type? **8,** 1–8
669 (2017).

670 31. Gasser, H. S. The classification of nerve fibers. *Ohio J. Sci.* (1941).

671 32. Tovote, P., Fadok, J. P. & Lüthi, A. Neuronal circuits for fear and anxiety. *Nat. Rev.*
672 *Neurosci.* **16,** 317–331 (2015).

673 33. Maren, S., Phan, K. L. & Liberzon, I. The contextual brain: implications for fear
674 conditioning, extinction and psychopathology. *Nat. Rev. Neurosci.* **14,** 417–428 (2013).

675 34. Yin, W. *et al.* A Central Amygdala–Ventrolateral Periaqueductal Gray Matter Pathway for
676 Pain in a Mouse Model of Depression-like Behavior. *Anesthesiology* **132,** 1175–1196
677 (2020).

678 35. Cleary, D. R., Neubert, M. J. & Heinricher, M. M. Are opioid-sensitive neurons in the rostral
679 ventromedial medulla inhibitory interneurons? *Neuroscience* **151,** 564–571 (2008).

680 36. Morgan, M. M., Whittier, K. L., Hegarty, D. M. & Aicher, S. A. Periaqueductal gray neurons
681 project to spinally projecting GABAergic neurons in the rostral ventromedial medulla. *Pain*
682 **140,** 376–386 (2008).

683 37. Ossipov, M. H., Dussor, G. O. & Porreca, F. Review series Central modulation of pain. **120,**
684 (2010).

38. Butler, R. K. *et al.* Molecular and electrophysiological changes in the prefrontal cortex-amygdala-dorsal periaqueductal grey pathway during persistent pain state and fear-conditioned analgesia. *Physiol. Behav.* **104,** 1075–1081 (2011).

39. McWilliams, L. A., Cox, B. J. & Enns, M. W. Mood and anxiety disorders associated with chronic pain: an examination in a nationally representative sample. *Pain* **106,** 127–133 (2003).

40. Courtin, J. *et al.* Prefrontal parvalbumin interneurons shape neuronal activity to drive fear expression. *Nature* **505,** 92–6 (2014).

41. Pérez-Escudero, A., Vicente-Page, J., Hinz, R. C., Arganda, S. & de Polavieja, G. G. idTracker: tracking individuals in a group by automatic identification of unmarked animals. *Nat. Methods* **11,** 743–748 (2014).

Acknowledgments

We thank Joshua Johansen, David Finn, and Nadine Gogolla for critical and stimulating discussions; K. Deisseroth and E. Boyden for generously sharing material, S. Laumond, J. Tessaire, and the technical staff of the housing and experimental animal facility of the Neurocentre Magendie. We thank Claire Francioni for her technical support. Microscopy was performed in the Bordeaux Imaging Center of the CNRS-INSERM and Bordeaux University, member of France BioImaging. This work was supported by grants from the French National Research Agency (ANR-FEARLESSPAIN, ANR-10-EQPX-08 OPTOPATH), the Fondation pour la Recherche Médicale (FRM-PhD grant to NW 2020-2021) and the French Society for the Study and Treatment of Pain (SFETD – grant to NW 2022).

Author Contributions

N.W performed behavioral experiments and optogenetic experiments on freely moving animals. F.A, J.V, performed electrophysiological and optogenetic experiments on anesthetized animals. E.V, L.C, N.W, F.A, Z.G, T.B, C.R, R.B, and D.G performed histology. N.W, M.L, S.V. P.F, and

712 C.H. designed the experiments. N.W, F.A, D.J, and E.V analyzed the data, N.W, D.J. and C.H
713 wrote the paper.

714

715 Supplementary Figures

716 **Supplementary Figure 1. Cued fear-conditioned analgesia behavior. a.** During habituation, the
717 freezing levels for the context (BL) and the two tones were low but significantly different (****, P
718 = 0.0003, Friedman test, n = 12 mice). **b.** Mean temperature at which the NC response was observed
719 in the HP test. The temperature of NC response was higher during CS^+ trials when compared to the
720 CS^- trials (***, P = 0.0005, Wilcoxon matched-pairs signed rank test, n = 12 mice)**. c.** Schematic
721 representation of how the back and tail temperature of the mice was measured. Every 30-sec three-
722 point temperature was taken for each of the two body parts. The temperature of the mice back and
723 tail were measured by the infrared digital thermographic camera and analyzed offline (see
724 Methods). The average temperature of the mice back (**d**) and tail (**e**) while the CS^+ or the CS^- were
725 presented. There were no differences in body temperature for the different CSs trials (ns, P > 0.05,
726 mixed-effects model, n = 13 mice). Vertical dashed lines correspond to the average time of NC
727 response for the CS^+ (red) and CS^- (blue) during the standard CFCA protocol.

728 **Supplementary Figure 2. CFCA depends on associative processes. a. Top**, protocol for the *No*
729 *Tone*: naïve mice were submitted to two HP trials without conditioning nor tone presentation.
730 **Bottom**, protocol for the *Tone*: naïve mice were submitted to two HP trials paired with an
731 unconditioned tone presentation. **b, c.** Mean latency and temperature of NC response for the two
732 tests mentioned above and the CFCA. The transient cued-fear induced analgesia (CS^+) compared
733 to the basal nociception, the tone, and the CS^- trials (***, P = 0.0001, Krustal-Wallis test). Trials

734 between the same type of test (*No tone* or *Tone*) were not significantly different (ns, P > 0.05,
735 Bonferroni post-hoc test, see statistical table for all comparisons) **d.** After fear extinction, there was
736 no difference in the mean temperature response between the two CSs (ns, P = 0.3276 paired t-test,
737 n = 10 mice). **e.** Protocol for stability training (see methods). Mice were submitted to two rounds
738 of the CFCA paradigm. During retrieval (**f, g**), average freezing values during CS^+ was higher than
739 CS^- or baseline (BL) periods (****, P < 0.0001, one-way RM ANOVA, n = 10 mice). **h, i.** Mean
740 latency and temperature of NC response during CS^- and CS^+ trials for FC HP test 1 (**h**) and test 2
741 (**i**). CS^+ presentation increased the latency and temperature of NC response in FC HP test 1 and test
742 2 (*, **, and ***, P < 0.05, paired t-test; for details, see supplementary table 1).

743 **Supplementary Figure 3. Two distinct neuronal populations in SST- Cre mice within the**
744 **PAG. a.** Representative picture of single-molecular fluorescent in situ hybridization for Sst
745 mRNAs in the PAG. Scale bar, 400 µm. **b, c.** Single-molecular fluorescent in situ hybridization for
746 Sst (green) and Cre (red) mRNAs in the vlPAG (left). Histograms showing the co-expression of
747 Sst/Cre as percentage of Sst-expressing cells (green) and as percentage of Cre-expressing cells
748 (red) in the dlPAG and vlPAG (right). Scale bar, 20 µm. **d.** Single-molecular fluorescent in situ
749 hybridization for Sst (red) and Slc32a1 (green) within the dlPAG (upper panel) and vlPAG (bottom
750 panel). Scale bar, 20 µm. **e.** Quantification of colocalization within the dlPAG (upper panel) and
751 vlPAG (bottom panel) of Sst^+ and $Slc32a1^+$. In the dlPAG approximately 19% of $Slc32a1^+$ cells
752 are Sst^+ and 17% of Sst^+ cells are $Slc32a1^+$. On the contrary, in the vlPAG approximately 95% of
753 $Slc32a1^+$ cells are Sst^+ and 61% of Sst^+ cells are $Slc32a1^+$. **f.** Single-molecular fluorescent in situ
754 hybridization for Sst (red) and Slc17a6 (green) within the dlPAG (upper panel) and vlPAG (bottom
755 panel). Scale bar, 20 µm. **g.** Quantification of colocalization within the dlPAG (upper panel) and
756 vlPAG (bottom panel) of Sst^+ and $Slc17a6^+$. In the dlPAG approximately 91% of $Slc17a6^+$ cells

757 are Sst^+ and 38% of Sst^+ cells are $Slc17a6^+$. On the contrary, in the vlPAG approximately 34% of
758 $Slc17a6^+$ cells are Sst^+ and 33% of Sst^+ cells are $Slc17a6^+$.White arrows indicate colocalization.

759 **Supplementary Figure 4. Comparable fear levels prior to the FC HP test**. After retrieval, fear
760 conditioning levels between the opsins and their respective GFP group was tested to ensure
761 equivalent fear levels. The discrimination index (see methods) between the GFP and ChR2 (**a**, ns,
762 P = 0.6052 unpaired t-test, n = 16 mice) or ArchT (**b,** ns, P = 0.4575, unpaired t-test, n = 23 mice)
763 were not significantly different. All the mice discriminated equally between CSs. The conditioning
764 index (see methods) between the GFP and ChR2 (**c,** ns, P = 0.2333, unpaired t-test n = 16 mice) or
765 ArchT (**d,** ns, P = 0.1320, unpaired t-test, n = 23 mice) were also not significantly different. All
766 mice displayed a similar high freezing level to the CS^+.

767 **Supplementary Figure 5. Optogenetic manipulation of SST^+ vlPAG cells does not affect**
768 **locomotion or produce aversion. a.** Photoactivation of SST^+ vlPAG cells abolished the analgesic
769 effect induced during defensive states (**, P = 0.0035, opsin x CS - two-way RM ANOVA, n = 7
770 GFP, n = 9 ChR2). The mean temperature of NC response for the CS^+ was significantly different
771 between the ChR2 and GFP groups (*, P = 0.0322, Bonferroni post-hoc test). For the ChR2 group,
772 the mean temperature of NC response during CS^+ was equivalent to the CS^- (ns, P = 0.1783,
773 Bonferroni post-hoc test). On the contrary, the mean temperature of NC response between the CSs
774 differed for the GFP group (****, P < 0.0001, Bonferroni post-hoc test). **b.** Photoinhibition of SST^+
775 vlPAG cells increased the analgesic effect for the ArchT group when compared to the GFP (**, P
776 = 0.0035, opsin x CS - two-way RM ANOVA, n = 12 GFP, n = 11 ArchT). The mean temperature
777 of NC response for the CS^- was significantly different between the ArchT and GFP groups (****,
778 P < 0.0001, Bonferroni post-hoc test). For the GFP group, the mean temperature of NC response
779 was higher for the CS^+ trials when compared to the CS^- trials (***, P = 0.0003, Bonferroni post-

780 hoc test), yet this was not the case for the ArchT group (ns, P > 0.999, Bonferroni post-hoc test).
781 **c.** The photoactivation of SST^+ vlPAG cells was performed during the ON epoch (blue shaded
782 area), and the average distance travelled during the ON epoch was not different from the OFF
783 epochs when comparing the two opsins (ns, P = 0.5121, opsin x light - two-way RM ANOVA, n =
784 7 GFP, n = 9 ChR2). **d.** The photoinhibition of SST^+ vlPAG cells was performed during the ON
785 epoch (yellow shaded area), and the average distance travelled during the ON epoch was not
786 different from the OFF epochs when comparing the two opsins (ns, P =0.4047, opsin x light - two-
787 way RM ANOVA, n = 12 GFP, n = 11 ArchT). **e.** Real-time place-preference location plot from a
788 representative animal while submitted to optogenetic activation of SST^+ vlPAG cells in the left
789 compartment throughout the 15-min session. **f**. There was no difference between ChR2- expressing
790 mice and the control group in the time spent on the stimulated and non-stimulated compartments
791 (ns, P = 0.1812, Mann Whitney test).

792 **Supplementary Figure 6. SST^+ vlPAG cells photoactivation during conditioning does not**
793 **impact fear learning. a**. Protocol for optogenetic manipulations during fear conditioning. On Day
794 2, mice received 5 CS-US associations. The US was either optogenetic stimulation alone or
795 optogenetic stimulation plus footshock. **b.** Average freezing levels during the CS-US association
796 of optogenetic stimulation alone. There was no difference in the overall freezing levels for the CS^-
797 and CS^+ between ChR2 and GFP (ns, P = 0.4804, opsin x CS - two-way RM ANOVA, n = 6 GFP,
798 n = 7 ChR2). **c.** During retrieval, there was no effect on freezing upon activation of SST^+ vlPAG
799 cells as an US (ns, P = 0.4804, opsin x CS effect - two-way RM ANOVA, n = 6 GFP, n = 7 ChR2).
800 **d.** Average freezing levels during the CS-US association of optogenetic stimulation plus footshock.
801 There was no difference in the overall freezing levels for the CS^+ and CS^- between ChR2 and GFP
802 (ns, P = 0.8663, opsin x CS effect - two-way RM ANOVA, n = 6 GFP, n = 7 ChR2). **e.** During

803 retrieval, there was no difference in the fear expression by the activation of the SST^+ vlPAG cells
804 (ns, P = 0.8967, opsin x CS effect - two-way RM ANOVA, n = 6 GFP, n = 7 ChR2).

805 **Supplementary Figure 7. Optogenetic effect observed during CFCA is not due to alteration**
806 **of somatostatin levels nor mediated by VIP^+ vlPAG cells. a**. Sst-IRES-Cre heterozygotic mice
807 received a bilateral injection of opsins in the vlPAG, and optic fibers were implanted above the
808 vlPAG. **b.** A representative example of expression patterns of ChR2 within SST^+ vlPAG cells. **c.**
809 Average freezing values during retrieval. ChR2 and GFP groups were pooled together because no
810 differences were found in the conditioning level (data not shown). The average freezing values
811 during CS^+ was higher than CS^- or baseline (BL) periods (****, P < 0.0001, Friedman test, n = 13
812 mice). **d.** Optogenetic activation of SST^+ vlPAG cells abolished the analgesic effect induced by
813 defensive states (**, P = 0.0048, opsin x CS - two-way RM ANOVA, n = 6 GFP, n = 7 ChR2).
814 The mean latency of NC response for the CS^+ was significantly different between the ChR2 and
815 GFP groups (*, P = 0.0300, Bonferroni post-hoc test, n = 6 GFP, n = 7 ChR2). For the ChR2 group,
816 the latency of NC response during CS^+ was equivalent to the CS^- (ns, P = 0.3342, Bonferroni post-
817 hoc test). On the contrary, the latency of NC response between the CSs was different for the GFP
818 group (****, P = 0.0001, Bonferroni post-hoc test). **e.** VIP-IRES-Cre mice received a bilateral
819 injection of opsins in the vlPAG, and optic fibers were implanted above the vlPAG. **f.**
820 Representative example of the expression pattern of ArchT within VIP^+ vlPAG cells. **g.** ArchT and
821 GFP groups were pooled together because no differences were found in the conditioning level (data
822 not shown). The average freezing values during CS^+ was higher than CS^- or BL periods (****, P <
823 0.0001, one-way RM ANOVA, n = 10 mice). **h.** Optogenetic inhibition of VIP^+ cells did not change
824 the analgesic effect for the ArchT group when compared to the GFP (ns, P = 0.5455, opsin x CS
825 effect - two-way RM ANOVA, n = 5 GFP, n = 5 ArchT). The latency of NC response was higher

826 for the CS^+ trials compared to the CS^- trials for both GFP and ArchT (***, $P < 0.01$, Bonferroni
827 post-hoc test, n = 5 GFP, n = 5 ArchT).

828 **Supplementary Figure 8. Optogenetic activation of SST^+ vlPAG cells did not affect tactile**
829 **sensitivity. a.** Perievent stimulus time histogram indicating the spiking latency of a purely tactile
830 neuron recorded in the spinal cord in response to gentle brushing of the skin. **b.** Representative
831 spiking activity latency of a purely tactile neuron recorded in the spinal cord in response to gentle
832 brushing of the skin with or without activation of ChR2 expressing SST^+ vlPAG cells. **c.** The
833 activation of ChR2 expressing SST^+ vlPAG cells of tactile neuron recorded in the spinal cord in
834 response to gentle brushing of the skin had no effect on the average firing activity (Paired t-test, P
835 = 0.6929, n = 5 cells).

836 **Supplementary Figure 9. Optogenetic manipulation of GFP expressing vlPAG cells did not**
837 **affect analgesia. a.** Single-unit recordings of WDR cells in the lumbar spinal cord during
838 optogenetic manipulation of GFP expressing SST^+ vlPAG inputs to the RVM. **b**. Photostimulation
839 of SST^+ vlPAG inputs to the RVM has no effect.

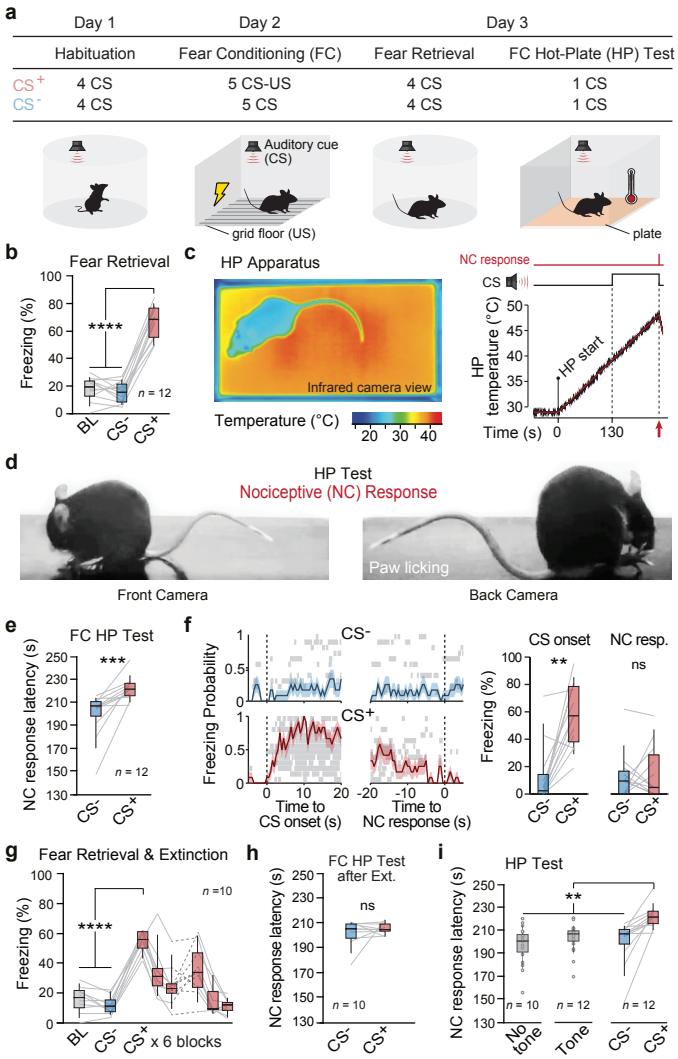

Winke et al., Figure 1

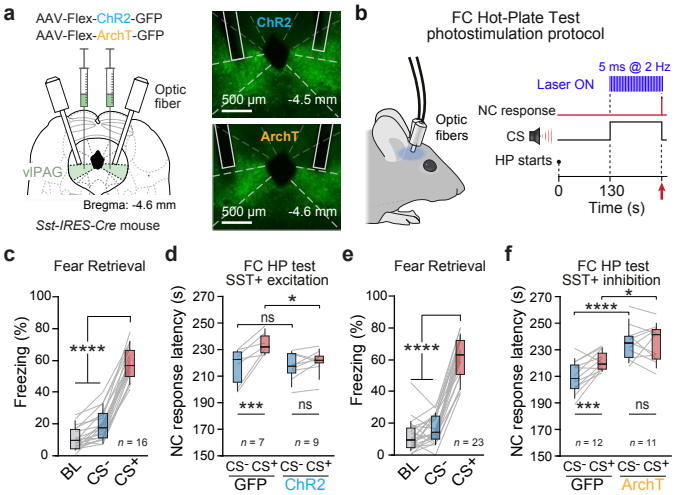

Winke et al., Figure 2

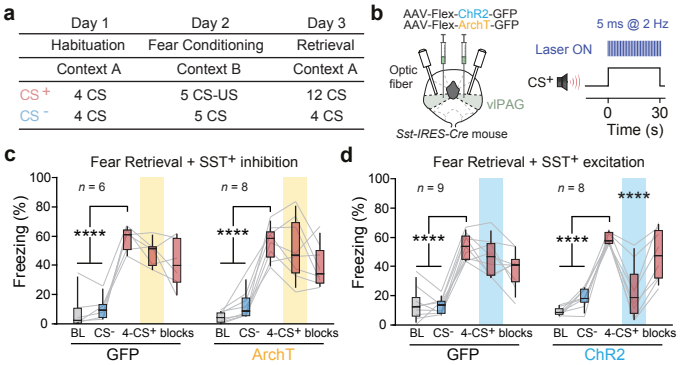

Winke et al., Figure 3

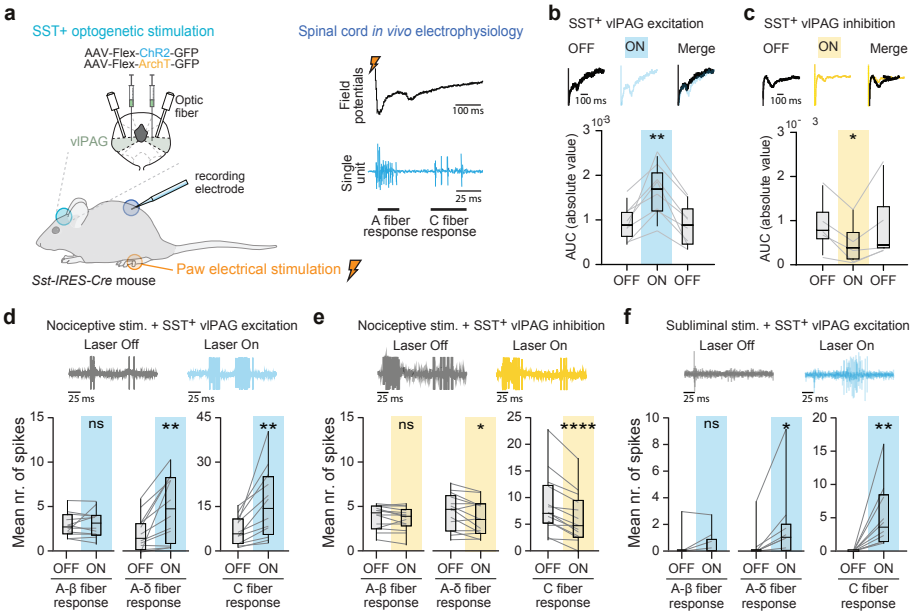

Winke et al, Figure 4

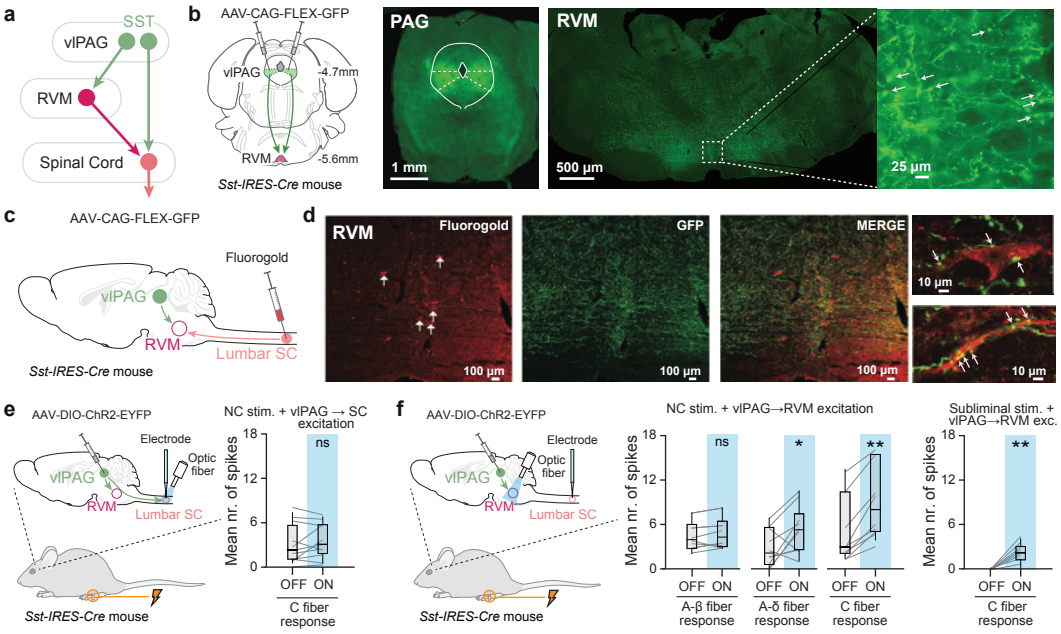

Winke et al., Figure 5

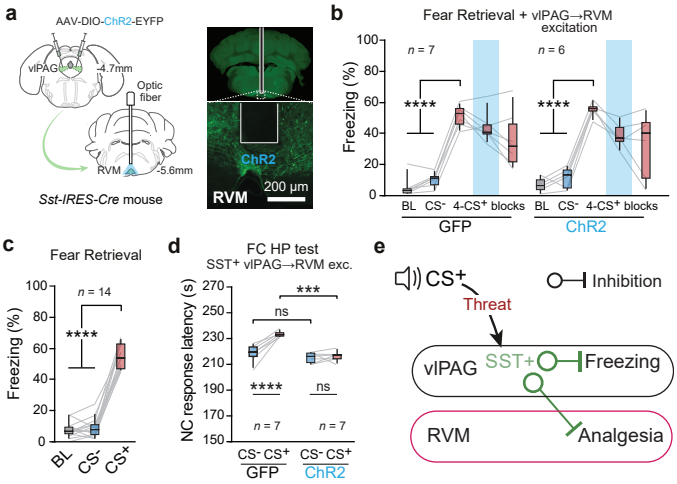

Winke et al., Figure 6